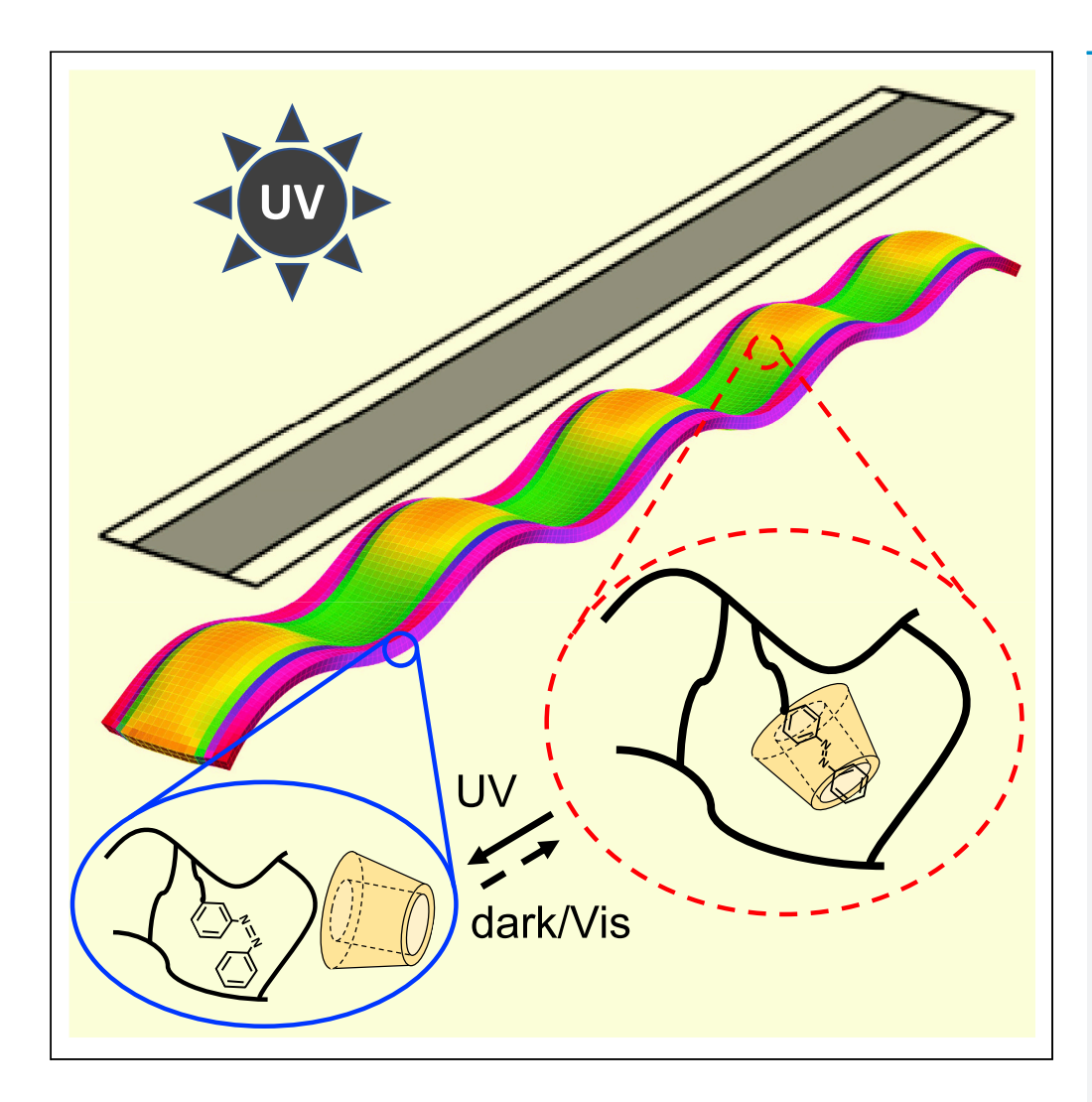


Article

Photocontrol of pattern formation and hysteresis loops in polymer gels with host-guest interactions



Yao Xiong, Olga Kuksenok

okuksen@clemson.edu

Highlights

Computational model captures dynamics of gels with host-guest interactions

Buckling patterns are observed in confined azobenzenefunctionalized gels

Patterns and hysteresis loops are controlled by non-uniform light illumination

Soft confinements are introduced by exposing selected regions of gel to UV light

Xiong & Kuksenok, iScience 25, 105606 December 22, 2022 © 2022 The Author(s). https://doi.org/10.1016/ j.isci.2022.105606





Article

Photocontrol of pattern formation and hysteresis loops in polymer gels with host-guest interactions

Yao Xiong¹ and Olga Kuksenok^{1,2,*}

SUMMARY

Patterns formed under external stresses are often critical for ensuring the functionality of soft materials. We focus on dynamic control of pattern formation and restructuring in hydrogels with host-guest interactions. We extend the three-dimensional gel Lattice Spring Model to capture the dynamics of photoresponsive hydrogels with pendant azobenzene moieties immersed in the α -cyclodextrin (α -CD) solution. While trans-azobenzene moieties are accommodated by the α -CD cavities forming inclusion complexes resulting in hydrogel swelling, exposure to UV irradiation induces trans-to-cis photoisomerization leading to decomplexation and matrix deswelling. We demonstrate swelling-induced patterns in confined samples upon adding the α -CD solution in the dark. Further, we show that spatiotemporal variations in UV irradiation effectively control patterns formed and hysteresis loops. We introduce soft confinements via illuminating specific regions of unconstrained samples with UV light. Our results indicate that features of patterns and hysteresis in systems' response to external conditions can be regulated via well-defined illumination patterns.

INTRODUCTION

Adaptability, compartmentalization, and growth are among well-recognized hallmarks of the living systems, which in turn inspire numerous efforts to mimic similar characteristics in fully synthetic materials. Pattern formation plays a vital role in many aspects of the above characteristics, contributing to the efficient functionality of living systems. The hydrogel matrix represents a soft responsive "canvas" that can be readily functionalized with various chemical moieties and reversible bonds to probe multiple aspects of out-of-equilibrium behavior of soft synthetic systems. Mechanical instabilities induced by sufficiently high compressive stresses in hydrogels undergoing swelling under various confinements result in the reconfiguration of the planar shape to out-of-plane patterns, such as wrinkling, buckling, creasing, and folding. Pecific confinements of hydrogels resulting in swelling-induced pattern formation under various conditions encompass clamping of gel edges, binding the gel to another elastic layer, 10,11 or introducing anisotropic swelling through the variation of gel properties.

Using light to control pattern formation and restructuring in hydrogels is of particular interest since illumination can be introduced remotely and non-invasively, and ideally can be applied numerous times to induce, erase, and rewrite patterns required for specific functionality. While imparting effective photoresponses can be challenging due to narrow ranges of operational conditions and fatigue during multiple switching cycles, a simple and facile approach to introduce robust photoresponses in hydrogels was recently proposed by Kuenstler et al. 18 by means of unitizing reversible host-guest complexation. Specifically, it had been shown 18 that gel swelling is effectively controlled by the isomerization state of incorporated azobenzene moieties and by the extent of complexation of these moieties with α -cyclodextrin (α -CD) units.

The azobenzene (Azo) moiety is a well-known and widely used photochemical group underdoing reversible interconversion between *trans*- and *cis*-conformations: the *trans*-to-*cis* photoisomerization is driven by the UV light irradiation, while the *cis*-to-*trans* isomerization occurs spontaneously via thermal relaxation in the dark and can also be induced by visible (Vis) light illumination. ^{19–21} The dynamics of the photoresponse and an extent of the equilibrium swelling under the UV light depends on how the azobenzene units are incorporated into the polymer network. ²² Specifically, due to more hydrophilic nature of *cis* isomers, an exposure to UV light can result in a moderate increase of linear swelling ratio of poly(*N*-isoproylacryamide)

¹Department of Materials Science and Engineering, Clemson University, Clemson, SC 29634, USA

https://doi.org/10.1016/j.isci. 2022.105606



²Lead contact

^{*}Correspondence: okuksen@clemson.edu



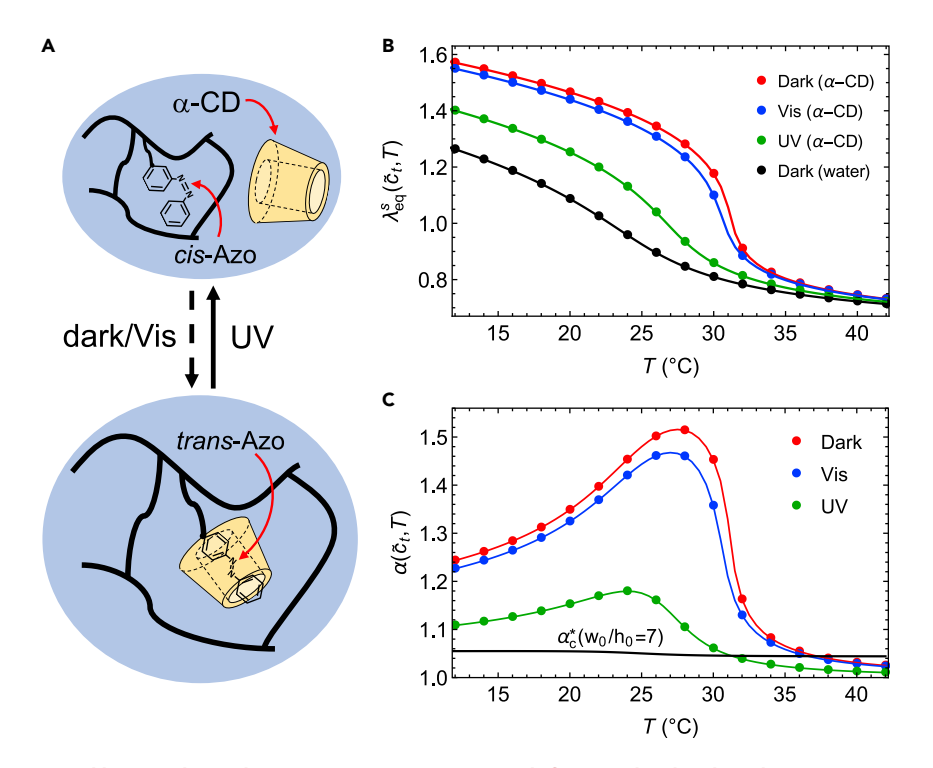


Figure 1. Equilibrium volume phase transitions in PNIPPAm gels functionalized with azobenzene moieties (A) Schematic of reversible complexation between azobenzene moieties grafted onto polymer strands in functionalized

(A) Schematic of reversible complexation between azobenzene moieties grafted onto polymer strands in functionalized PNIPPAm gels and α -CD units dissolved in water. The *cis*-to-*trans* photoisomerization of azobenzene moieties results in the complexation resulting in swelling of the polymer matrix, while the *trans*-to-*cis* transition leads to decomplexation and correspondingly shrinking of the hydrogel.

(B) Equilibrium degree of swelling, $\lambda_{eq}^s(\tilde{c}_t,T)$, for hydrogels in pure water in the dark ($\lambda_{eq}^w(\tilde{c}_t,T)$, in black), and hydrogels in the α -CD solution, $\lambda_{eq}^{\alpha\text{-CD}}(\tilde{c}_t,T)$, in the dark, under UV light irradiation, and under visible light irradiation (in red, in green, and in blue, respectively).

(C) Equilibrium swelling ratio of hydrogels, $\alpha(\bar{c}_t,T)$, in aqueous α -CDs solution in the dark (in red), under UV irradiation (in green), and under visible light irradiation (in blue). At each temperature, the swelling ratio is calculated as a ratio between the equilibrium degree of swelling at conditions listed above, $\lambda_{\rm eq}^{\alpha - CD}(\bar{c}_t,T)$, and that in pure water in the dark, $\lambda_{\rm eq}^{w}(1,T)$. The black line is the analytical prediction of the critical swelling ratio, $\alpha_{\rm c}^*(w_0/h_0)$, above which the flat hydrogel film with two clamped edges loses in-plane stability; w_0 and h_0 are the initial width and thickness of the sample in pure water in the dark. In (A and B), the filled circles are simulation results and the lines of the corresponding color represent analytical calculations.

(PNIPAAm) hydrogels with azobenzene pendant groups. ^{18,23,24} On the contrary, a decrease in the swelling ratio upon UV irradiation was observed in the PNIPAAm hydrogels with crosslinks incorporating azobenzene groups, ²⁵ the latter effect was attributed to the decrease in entropy of polymer chains during the *trans*-to-*cis* photoisomerization.

While the nearly planar *trans*-azobenzene (*trans*-Azo) moieties can be recognized and efficiently accommodated by the cavities of cyclodextrins (CDs) to form inclusion complexes (Figure 1A), an exposure to UV irradiation drives the *trans*-to-*cis* photoisomerization and causes the dissociation of the complexes. ^{26–29} Utilizing these host-guest interactions, the photo-responsive behavior of azobenzene-functionalized hydrogel-based systems can be substantially modulated and often amplified by dissolving free CDs units in water ^{18,30} or by integrating CDs as physical crosslinkers. ^{31,32} If the gel is physically crosslinked via the host-guest interactions in addition to the chemical crosslinking, then UV/Vis irradiation induces an expansion-contraction behavior, not a sol-gel phase transition. ^{31,32}

Herein, we focus on modeling PNIPAAm hydrogels with pendant azobenzene moieties immersed in water with dissolved α -CD units as shown in Figure 1A. We begin with extending three-dimensional gel lattice spring model (3D gLSM)³³ to be able to capture the dynamics of the hydrogels with pendant Azo groups

iScience Article



immersed into the α -CD solution. We first demonstrate that the proposed model reproduces volume phase transitions in azobenzene-functionalized hydrogels with host-guest interactions and related reconfiguration of the shapes of thin hydrogel sheets under non-uniform light as reported in the recent experimental study. ¹⁸ We then demonstrate the buckling of thin hydrogel films under rigid confinement upon immersion of the hydrogel film with long edges clamped into the α -CD solution. Further, we utilize variations in light irradiation conditions to control pattern formation in thin hydrogel films under rigid and soft confinements and to control hysteresis in hydrogel response to changes in external environments. Soft confinement is introduced via illuminating specific regions of the thin samples with UV light; this patterned illumination introduces localized regions with higher rigidity. While significant progress had been made in understanding swelling-induced pattern formation in various confined hydrogels, ^{7,10,11,34–38} herein pattern formation and hysteresis loops are modeled in the hydrogels with host-guest interactions. Our results show that an onset of buckling and specific features of patterns formed along with hysteresis in systems' response to external conditions can be effectively controlled in polymer networks with host-guest interactions via well-defined illumination patterns.

RESULTS

Adapting the gel lattice spring model framework to model hydrogels with host-guest interactions

The gel Lattice Spring Model (gLSM) approach was originally developed to simulate dynamics of the chemo-responsive gels undergoing Belousov-Zhabotinsky chemical reactions (referred to as BZ gels) in two^{39,40} and in three³³ dimensions. The results obtained using gLSM are in a good agreement with a number of experimental findings. 41-47 The gLSM was further extended to model the photo-response of BZ gels⁴⁸⁻⁵⁴ and dynamics of the spyrobenzopyran-functionalized gels.^{55,56} In this work, we adapt three-dimensional gel Lattice Spring Model (3D gLSM)^{33,45} to capture the dynamics of the azobenzene-functionalized PNIPAAm hydrogels immersed into the α -CD solution under UV irradiation and under the visible light. The details of 3D gLSM approach are introduced in the computational methods section later in discussion. The approach proposed herein captures the UV-driven trans-to-cis photoisomerization of the pendent azobenzene groups and the expulsion of the chromophores in their cis-form (cis-Azo) from the α -CD cavities, which causes the decrease in the hydrophilicity of the polymer matrix. The proposed model also accounts for the cis-to-trans isomerization under visible light or due to the thermal relaxation and corresponding formation of the host-guest supramolecular complexes between the trans-azobenzene moieties and α -CD units. ⁵⁷⁻⁵⁹ The models capturing the isomerization of azobenzene moieties typically consider three processes: UV-driven trans-to-cis photoisomerization, the visible light-driven cis-to-trans photoisomerization, and the spontaneous trans-to-cis thermal relaxation as following $^{19,60-63}$:

$$k_{tc}$$
 $trans$ -Azo $\rightleftharpoons cis$ -Azo (Equation 1)
 k_{ct}, k_t

where $k_{\rm tc}$ and $k_{\rm ct}$ are the rate constants of the *trans*-to-*cis* and *cis*-to-*trans* photoisomerization, respectively, which can be controlled by the intensity and the wavelength of light, and $k_{\rm t}$ is the rate of spontaneous thermal *cis*-to-*trans* relaxation. The association and dissociation of the azobenzene moieties with

$$k_a$$
 the α-CD units, trans-Azo+α-CD \rightleftharpoons trans-Azo@α-CD, where k_a and k_d are the association and dissocia-

tion rate constants, respectively, had been shown to occur significantly faster than the photoisomerization. 60,64 Specifically, the isomerization of the azobenzene had been demonstrated to be the rate-limiting reactive process and the complexation with the α -CD units had been shown not to affect the photostationary state of the azobenzene-functionalized surface. 64 Further, in the recent study of the photokinetics of the supramolecular Azo/CD complexes, the dissociation of the Azo compound from the complexes was considered to occur simultaneously with the isomerization kinetics. 60 Hence, we assume that the photoisomerization is the rate-limiting reaction process and that the complexation/decomplexation occurs simultaneously with the isomerization. We also assume that all pendant *trans*-azobenzene moieties form inclusion complexes with free α -CD units with the stoichiometry of $^{57-59}$ 1:1, this assumption is valid provided that an excess amount of the α -CD units is available for the complexation. 60 Thereby the concentration of the inclusion complexes is assumed to be equal to the concentration of the azobenzene





moieties in trans conformation (trans-Azo), c_t , in the presence of the α -CD units dissolved in water, and follows the reaction kinetics corresponding to Equation 1 above: 62,63

$$\frac{\mathrm{d}c_{t}}{\mathrm{d}t} = -k_{tc}c_{t} + (k_{ct} + k_{t})(1 - c_{t})$$
 (Equation 2)

The value of c_t in Equation 2 is normalized by the total concentration of azobenzene pendent groups grafted onto the polymer matrix. The values of rate constants k_{ct} , k_{tc} , and k_t are assumed to be independent on temperature within the temperature range probed in this study. Finally, we consider only relatively thin samples (of the thickness up to $\sim 30~\mu m$ as shown later in discussion). This thickness is smaller than the penetration depth of the UV light, ¹⁸ leading to an approximately uniform light absorption and constant values of k_{ct} and k_{tc} through the sample thickness. For the uniformly illuminated thin sample, the time evolution of the azobenzene moieties in *trans* conformation follows $c_t(t) = \tilde{c}_t + (c_t(0) - \tilde{c}_t) \exp(-t/\tau)$, where $c_t(0)$ is the initial value and $\tilde{c}_t = (k_{ct} + k_t)\tau$ is the photostationary concentration of *trans*-Azo normalized on the total concentration of Azo moieties grafted onto the polymer network, and $\tau = (k_t + k_{ct} + k_{tc})^{-1}$ is the respective photorelaxation time.

Within the framework of gLSM,⁴⁰ the total energy of the deformed polymer network encompasses mixing energy and elastic energy contributions. The dimensionless mixing energy normalized by k_BT , where k_B is the Boltzmann constant, can be written as⁶⁵:

$$U_{\text{FH}} = \sqrt{I_3}[(1-\varphi)\ln(1-\varphi) + \chi_{\text{FH}}(\varphi, T)\varphi(1-\varphi) + f_{\text{int}}(\varphi, c_t)]$$
 (Equation 3)

The first two terms on the right-hand side of Equation 3 correspond to the mixing energy of PNIPAAm hydrogels with all pendant azobenzene moieties in the *trans*-state in pure water, φ is the polymer volume fraction, and $\chi_{\rm FH}(\varphi,T)$ is the polymer-solvent interaction parameter. $I_3=\det\widehat{\bf B}$ in Equation 3 is an invariant of the left Cauchy-Green (Finger) strain tensor $\widehat{\bf B}$; $I_3^{1/2}$ is the volume change with respect to the volume at preparation. One in Equation 3, $I_{\rm int}(\varphi,c_t)$, accounts for the contributions due to the photoisomerization of the azobenzene derivatives and the complexation in the presence of the α -CD units dissolved in water. An effect of the oxidized catalyst grafted onto the polymer matrix on the swelling of the chemoresponsive gels was introduced within the original gLSM framework in a similar manner. Specifically, an additional term was incorporated in the Flory-Huggins mixing energy proportional to the volume fraction of the catalyst in the oxidized state, C_V , as $S^{39,40} - \chi^* C_V (1-\varphi)$, where $\chi^* > 0$ represented a fitting parameter corresponding to the strength of the effect. Further, the effects of the spirobenzopyran chromophores on the swelling of polymer networks in acidic aqueous solution were introduced within the gLSM framework via the incorporation of the additional term in mixing energy proportional to the concentration of the chromophores in their spiro form. Adapting the same approach, we introduce the last term in Equation 3 as

$$f_{\text{int}}(\varphi, c_t) = -\beta_1 (1 - \varphi)(1 - c_t) - \beta_2 (1 - \varphi)c_t$$
 (Equation 4)

The first contribution in Equation 4 captures the effects of the interaction of polymer chains with pendent cis-Azo moieties with pure water in the absence of the α -CD units; this contribution results in a moderate swelling of the polymer matrix under UV irradiation. The second contribution in Equation 4 is due to the complexation of the pendant trans-Azo moieties in the presence of the α -CD units, this contribution promotes distinct swelling of the hydrogel in the dark or in visible light; $\beta_2=0$ in pure water in the absence of α -CD. The parameters β_1 and β_2 (both positive values) introduce the strengths of the corresponding effects and are considered fitting parameters of the model proposed herein. The second contribution to the total energy is the dimensionless elastic energy of the crosslinked polymer network 67 $U_{\rm el}$ (see more details in the computational methods section later in discussion).

An equilibrium is reached at a chosen temperature when the contributions from the elastic and mixing stresses to the total stress are balanced ($\hat{\sigma} = 0$, more details are provided in the computational methods section later in discussion), and the fraction of trans-Azo moieties reaches its photostationary state, $\tilde{c}_t = \frac{k_t + k_{ct}}{k_t + k_{ct} + k_{tc}}$. Thereby, an equilibrium degree of swelling for the three-dimensional unconstrained sample freely swollen in the solvent can be calculated analytically as

$$\lambda_{\text{eq}}^{\text{s}}(\tilde{c}_{\text{t}}, T) = \left(\frac{\varphi_0}{\varphi_{\text{eq}}^{\text{s}}(\tilde{c}_{\text{t}}, T)}\right)^{\frac{1}{3}}$$
 (Equation 5)

at a given \tilde{c}_t and temperature T; the superscript "s" denotes the type of solvent, so that $\lambda_{ea}^w(\tilde{c}_t, T)$





Illumination	k_{tc}	k_{ct}	k_t	\tilde{c}_t
UV	$2.0 \times 10^{-2} \text{ s}^{-1} (4.0 \times 10^{-3})$	$7.0 \times 10^{-3} \text{ s}^{-1} (1.4 \times 10^{-3})$	$2.0 \times 10^{-5} \text{ s}^{-1} (4.0 \times 10^{-6})$	0.260
Vis	$1.0 \times 10^{-3} \text{ s}^{-1} (2.0 \times 10^{-4})$	$1.0 \times 10^{-2} \text{ s}^{-1} (2.0 \times 10^{-3})$	$2.0 \times 10^{-5} \text{ s}^{-1} (4.0 \times 10^{-6})$	0.909
Dark	$0 s^{-1} (0)$	$0 s^{-1} (0)$	$2.0 \times 10^{-5} \text{ s}^{-1} (4.0 \times 10^{-6})$	1

and $\lambda_{\rm eq}^{\alpha\text{-CD}}(\tilde{c}_t,T)$ refer to the equilibrium degree of swelling in pure water and in the α -CD solution, respectively. The equilibrium volume fraction of polymer for a given solvent type $\varphi_{\rm eq}^{\rm s}(\tilde{c}_t,T)$ is found by solving 33

$$c_0 \left[\left(\frac{\varphi_{\text{eq}}^s}{\varphi_0} \right)^{1/3} - \frac{\varphi_{\text{eq}}^s}{2\varphi_0} \right] \ = \ - \ \left[\varphi_{\text{eq}}^s + \ln \left(1 - \varphi_{\text{eq}}^s \right) + \chi \left(\varphi_{\text{eq}}^s, T \right) \varphi_{\text{eq}}^{s-2} \right] \ + \ c_0 \frac{\varphi_{\text{eq}}^s}{2\varphi_0} + \ \beta_1 (1 - \tilde{c}_t) + \beta_2 \tilde{c}_t \right] + c_0 \frac{\varphi_{\text{eq}}^s}{2\varphi_0} + \beta_1 (1 - \tilde{c}_t) + \beta_2 \tilde{c}_t + \beta_1 (1 - \tilde{c}_t) + \beta_1 \tilde{c}_t + \beta_1 \tilde{c}_t + \beta_2 \tilde{c}_t + \beta_1 \tilde{c}_t + \beta_2 \tilde{c}_t + \beta_1 \tilde{c}_t + \beta_2 \tilde{c}_t + \beta_2 \tilde{c}_t + \beta_1 \tilde{c}_t + \beta_2 \tilde{c}_t + \beta$$

(Equation 6)

where \tilde{c}_t is calculated based on the respective reaction constants (Table 1), and $\beta_2 = 0$ in pure water (more details are provided in the computational methods section later in discussion).

Defining system parameters and calculating the equilibrium degree of swelling

The reference sample size chosen in our simulations is 200×15×3 nodes unless specified otherwise. We choose the dimensionless crosslink density and volume fraction of polymer at preparation as $c_0 = 2.6 \times 10^{-3}$ and $\varphi_0 = 0.21$, respectively, based on the available data from the experimental study. 18 We first calculate the equilibrium degree of swelling of the PNIPAAm hydrogel with all pendant azobenzene moieties in trans-state in the absence of the α -CD units as a function of temperature; to do so, we set $c_t = 1$ and $\beta_1 = \beta_2 = 0$ in Equation 6. The polymer-solvent interaction parameter can be expressed as $^{68}\chi(\varphi,T)=\frac{\Delta H-T\Delta S}{k_{\Phi}T}+\chi_{1}\varphi$, where ΔS and ΔH represent the entropy and enthalpy change during mixing, respectively; the values of ΔS , ΔH , and χ_1 are often treated as fitting parameters to reproduce experimentally available data. 25,69 In the simulations later in discussion, we set $\Delta S = -4.717 \text{ x}$ 10^{-23} J/K, $\Delta H = -1.198 \times 10^{-20}$ J and $\chi_1 = 0.33$; while ΔS is set as provided in Ref. 68, ΔH and χ_1 represent the best fit corresponding to the minimum of the mean absolute error with respect to the available experimental data on the equilibrium degree of swelling of PNIPAAm hydrogel with all pendant azobenzene moieties in trans-state in pure water. 18 Specifically, the data points from the experimental study (marked by black stars in Figure S1 in supplemental information) are recalculated from the data available in Ref. 18 for the areal swelling ratio of PNIPAAm hydrogels in pure water (no α -CD units) in the dark and are used to find the best fit for ΔH and χ_1 . Wolfram Mathematica software 70 was used to perform the fitting and to generate all the plots and morphology snapshots below. Notably, the incorporation of pendent azobenzene groups causes an increase in ΔH with respect to that of pure PNIPAAm network⁶⁸; similar trends in ΔH due to the incorporation of azobenzene moieties were also observed in poly(N-vinylcaprolactam) (PVCL) microgels⁷¹ and in PNIPAAm with azobenzene crosslinking.²⁵

Since the absorption spectra of *trans* and *cis* isomers of azobenzene moieties overlap substantially, a single wavelength of light can activate both forward and reverse photoisomerzation and results in a mixed photostationary state: maximum of approximately 80% *cis*-Azo upon UV light or 95% *trans*-Azo upon visible light. ^{18,58,72} We select the reference values of rate constants as listed in Table 1. These values are chosen within the range for the photoisomerization and thermal relaxation of azobenzene derivatives incorporated into the polymers, specifically within the range of $10^{-4} \sim 10^{-2} \, \text{s}^{-1}$ for k_{tc} and k_{ct} (Ref. 73-81), and $10^{-6} \sim 10^{-4} \, \text{s}^{-1}$ for k_t (Ref. 18,82-86). At the values of reaction rate constants chosen (Table 1), the photostationary concentrations of azobenzene units in *trans*-Azo are $\tilde{c}_t = 0.260$ upon UV illumination and $\tilde{c}_t = 0.909$ upon visible light irradiation, which are within the range provided in Ref. 18, where a photostationary concentration of >70% of *cis*-Azo is achieved upon illumination with 50 mW cm⁻² of 365 nm light. Notably, we chose $k_t \ll k_{ct}$, so that the thermal relaxation in the dark back to the *trans*-azobenzene occurs significantly slower than the same process under the visible light, similar to that in the respective experimental study. ¹⁸





To calculate the fitting parameters β_1 and β_2 , we selected the photostationary concentrations in the respective cases (in pure water and in the α -CD solution) and calculated the best fit to the respective swelling ratio measured in experiments ¹⁸ at a range of temperatures in two cases: under UV light irradiation in pure water ($\tilde{c}_t = 0.260$) and in the dark in α -CD solution ($\tilde{c}_t = 1$), respectively. Using the values of ΔS , ΔH_{i} and χ_{1} listed above, the best fit corresponding to the minimum mean absolute error was found at $\beta_1 = 5.0 \times 10^{-3}$ and $\beta_2 = 1.735 \times 10^{-2}$. We set our dimensionless unit of length and time to $L_0 = 10 \, \mu \text{m}$ and $T_0 = 0.2 \, \text{s}$, respectively. In the estimates, the collective diffusion coefficient is taken as 87 2×10^{-11} m²/s. With these time and length scales, the characteristic diffusion time for a cubic sample $(3\times3\times3$ nodes, the dimensional size 27.4 μ m \times 27.4 μ m \times 27.4 μ m) upon equilibrium under UV light irradiation is 36.4 s (initially, the sample is in the dark at 25°C, Figure S2A), and the characteristic thermal relaxation time in pure water at 25°C is 13.9 h (Figure S2B). Both characteristic relaxation times are in agreement with the experimental results, where the characteristic relaxation time under UV light irradiation at room temperature for the hydrogel of a similar size initially in the dark in the α -CD solution is about 30 s, and the thermal relaxation time is about 15h. 18 Our simulations also reproduce the shape morphing of the thin gel samples suspended in the α -CD solution provided that selected portions of these samples are exposed to UV irradiation (Figures S2CD), similar to that demonstrated in the previous experimental study. 18 In what follows, all the dimensionless values of time and length are provided in units of T_0 and L_0 , respectively.

Equilibrium degree of swelling of azobenzene-functionalized poly(N-isoproylacryamide) hydrogels in water and in α -cyclodextrin solution

We first calculate the equilibrium degree of swelling of free (unconstrained) hydrogels in pure water in the dark, $\lambda_{eq}^{w}(\tilde{c}_{t},T)$, (in black in Figure 1B), and the equilibrium degree of swelling of unrestricted hydrogels in the α -CD solution, $\lambda_{eq}^{\alpha\text{-CD}}(\tilde{c}_{t},T)$, under the following conditions: in the dark (in red), under UV irradiation (in green), and under visible irradiation (in blue in Figure 1B). The filled circles of the corresponding color mark the data points calculated from the 3D gLSM simulations; in these runs, the degree of swelling was calculated upon free (unconstrained) samples (3×3×3 nodes) reaching an equilibrium under respective conditions. The solid lines of the same color denote corresponding analytical calculations (Equation 7 with φ_{eq}^{s} given by Equation 8) and show an excellent agreement between analytical predictions and data points obtained from 3D gLSM simulations.

It is instructive to calculate the ratio of the equilibrium degree of swelling for the free samples in the α -CD solution under various conditions to that in pure water in the dark, $\alpha(c_t, T) = \lambda_{eq}^{\alpha \text{-CD}}(c_t, T)/\lambda_{eq}^w(1, T)$. Figure 1 clearly shows that adding aqueous α -CD units in the dark results in the pronounced swelling of hydrogels upon reaching an equilibrium at all the temperatures considered with the highest peak value in $\alpha(\tilde{c}_t, T)$ (red curves in Figure 1). UV irradiation enables trans-to-cis photoisomerization, which in turn leads to the dissociation of a large fraction of the host-quest complexes and decreasing the fraction of trans-Azo moieties upon reaching the photostationary concentration ($\tilde{c}_t = 0.260$ under UV). Correspondingly under UV irradiation, the equilibrium degree of swelling of the hydrogel placed into the α -CD solution decreases at all temperatures, and the volume phase transition becomes more gradual with the transition temperature shifted to the left (compare green and red curves in Figure 1). These both trends closely correspond to the trends in the respective prior experimental study. 18 Further, we also considered the effects of illumination with visible light (in green in Figure 1). As discussed above, the visible light irradiation enables both cisto-trans and trans-to-cis photoisomerization, resulting in the dissociation of a relatively small fraction of the host-guest supramolecular complexes (photostationary concentration is $\tilde{c}_t = 0.909$ under visible irradiations, see Table 1). Since the value of \tilde{c}_t in this scenario is close to that in the dark ($\tilde{c}_t = 1.0$), the volume phase transition and equilibrium swelling ratio resemble that in the dark with correspondingly small decrease in $\lambda_{ea}^{\alpha\text{-CD}}(\tilde{c}_t, T)$ and $\alpha(\tilde{c}_t, T)$ for all temperatures (blue curves in Figure 1) with respect to the same values in the dark. This scenario is of interest in our studies of the dynamic response of the hydrogel to illumination conditions.

Dynamic control of pattern formation in hydrogels with host-guest interactions

We next focus on the effect of varying illumination conditions on pattern formation in confined hydrogels. As two reference cases, we choose the samples initially in the pure water in the dark at two temperatures, 20° C and 33° C. In these two scenarios, we first constrain the reference sample ($200 \times 15 \times 3$ nodes) by



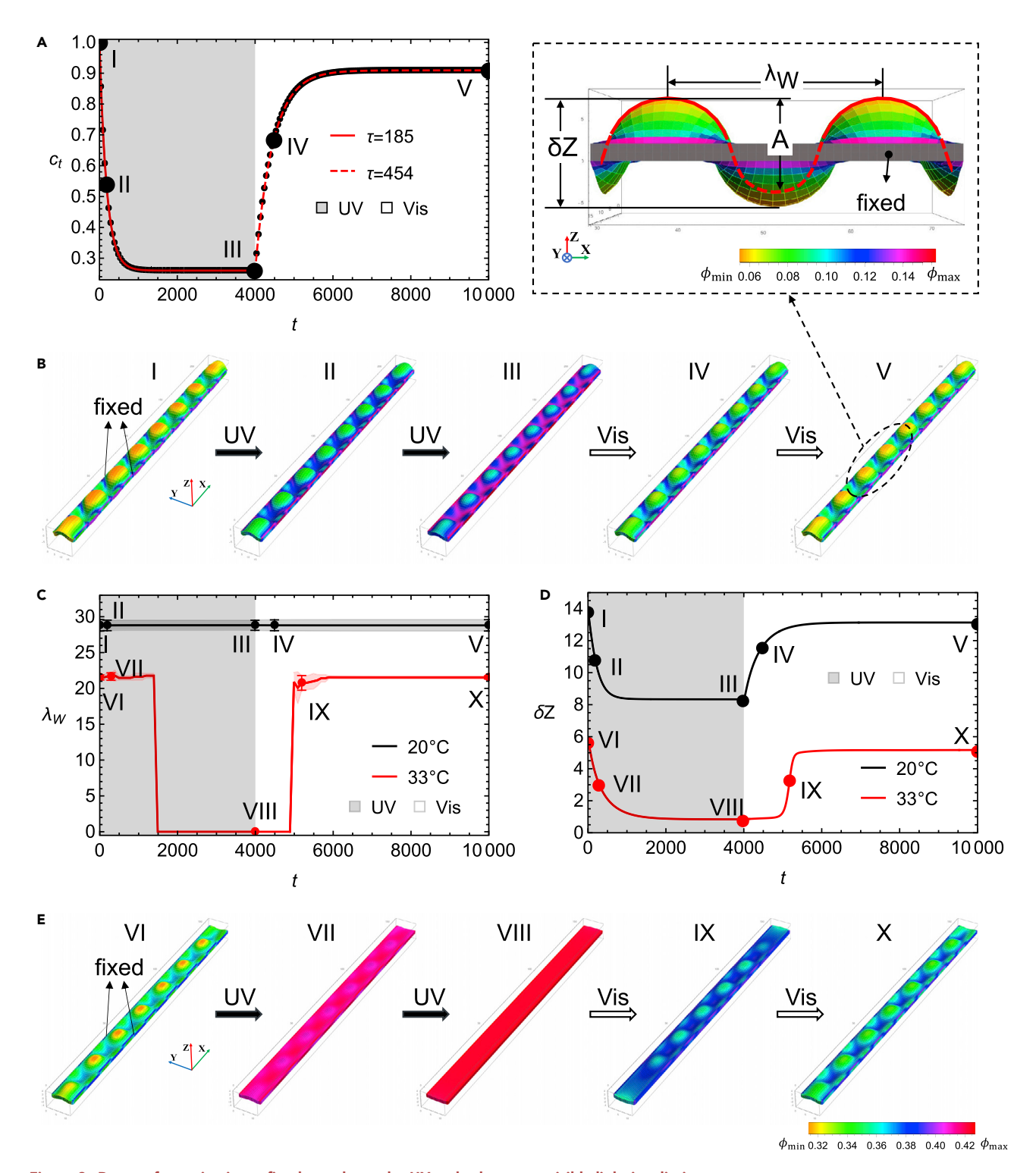


Figure 2. Pattern formation in confined samples under UV and subsequent visible light irradiations

(A) Time evolution of the fraction of trans-Azo, c_t , for the confined sample under UV light irradiation (gray shaded region), followed by visible light irradiation (white region) at 20°C. The solid and dashed red lines correspond to the analytical solution for $c_t(t)$, where $c_t(0) = 1$ and $\tau = 185$ in the shaded region and $c_t(0) = 0.26$ and $\tau = 454$ in the remaining portion of the plot; the values of k are given in Table 1.





Figure 2. Continued

(B) Snapshots of the sample morphology at five time instances (marked I-V in (A)). The inset (top right) represents the cross-section of the sample taken along the central node in the y-direction.

(C and D) Time evolution of the wavelength (in C) and the amplitude (in D) for the samples at 20°C (in black) and 33°C (in red), correspondingly. (E) The snapshots of the sample morphology at selected time instances (marked IV-X in (C and D)) at 33°C. The color in (B and E) corresponds to the local polymer volume fraction as represented by the respective color bars.

holding the position of two long edges. The respective equilibrium degree of swelling at initial conditions is calculated analytically as detailed above; see also Figure 1B (black curve) for $\lambda_{eq}^{w}(1,20^{\circ}\text{C})$ and $\lambda_{eq}^{w}(1,33^{\circ}\text{C})$ at equilibrium in the dark. These calculated values of λ_{eq}^{w} result in the initial dimensional sample sizes of 2.16 mm×0.15 mm×0.022 mm (at 20°C) and 1.54 mm×0.11 mm×0.015 mm (at 33°C), respectively.

Our recent study showed that a flat hydrogel membrane confined at two long edges loses in-plane stability and exhibits pattern formation upon swelling, provided that the swelling ratio α exceeds the threshold value. For the infinitely long sample with the initial thickness-to-width aspect ratio h_0/w_0 , the linear stability analysis results in the following estimate of the threshold value of the swelling ratio

$$\alpha_c^* = \left[1 - \frac{3.09}{1+v} \left(\frac{h_0}{w_0}\right)^2\right]^{-1}$$
, where v is the Poisson's ratio. The swelling ratio here is defined as the ratio of

the equilibrium degree of swelling of free (unrestricted) swollen sample with respect to that corresponding to the initial conditions (flat morphology). In Figure 1C, black line corresponds to α_c^* for azobenzene-functionalized hydrogels with $w_0/h_0=7$; see Figure S3A for the Poisson's ratio of the gel as a function of temperature. Hence, the buckling instabilities are anticipated if the swelling ratio exceeds α_c^* . For $\alpha(\tilde{c}_t,T)<\alpha_c^*$, the confined sample is expected to remain approximately flat (no patterns formed) for these moderate degrees of swelling (see Figure S3B).

As anticipated from the above discussion, the patterns develop at late times at both chosen temperatures (20°C and 33°C) upon equilibration after the addition of the α-CD solution in the dark (Figure S4) since the condition $\alpha(\tilde{c}_t, T) > \alpha_c^*$ holds. We now place the buckled sample equilibrated in the α -CD solution at 20°C under the UV light irradiation for a time interval of $\Delta t = 4 \times 10^3$, and then under the visible light irradiation for a time interval of $\Delta t = 6 \times 10^3$. Figure 2A shows the time evolution of the fraction of Azo moieties in the trans state, c_t , for the confined sample under UV light irradiation (gray shaded region), followed by visible light irradiation (white region) at 20°C. The time intervals of the respective applied illumination are chosen to be sufficiently long such that ct reaches the respective photostationary state and remains in this state for a prolonged time. UV irradiation results in the trans-to-cis photoisomerization and dissociation of a large fraction of inclusion complexes, so that the fraction of trans-Azo moieties, c_t , decays with the relaxation time of $\tau = 1/(k_{tc}(UV) + k_{ct}(UV) + k_t) = 185$. Correspondingly, we find that the average volume fraction of polymer, $\langle \varphi \rangle$, increases, which corresponds to the solvent expelled from the polymer matrix. The subsequent visible irradiation results in the cis-to-trans photoisomerization and correspondingly re-association of the inclusion complexes, so that the fraction of trans-Azo moieties, c_t , increases with the relaxation time of $\tau = 1/(k_{tc}(Vis) + k_{ct}(Vis) + k_t) = 454$. The simulation snapshots at five selected time instants marked in Figure 2A are shown in Figure 2B, the color represents the local volume fraction of the polymer according to the color bar.

To characterize pattern formation and restructuring under UV or visible illumination, we calculate the amplitude δZ as the distance between the highest and the lowest z-coordinates of the centers of the elements, and the wavelength λ_W as the distance between the two neighboring peaks along the sample length (see inset in Figure 2B). To minimize effects of the free edges, we exclude 5% of total elements at each short end of the sample when calculating δZ and λ_W . The wavelength λ_W is calculated when the amplitude of the surface undulations exceeds $0.1h_0$ and two or more wavelengths fit within the length of the sample, this value is averaged over the length of the sample. We track the time evolution of λ_W (in black in Figure 2C) and δZ (in black in Figure 2D). The sample at 20° C remains buckled during both UV and visible light irradiations. Our results show that the wavelength remains approximately constant at $\lambda_W = 28.8 \pm 0.8$ during all stages (in black in Figure 2C), while variations in the transient and equilibrium degrees of swelling due to UV and Vis irradiations result in distinct variation of the amplitude δZ (in black in Figure 2D).

The time evolution of λ_W and δZ for the confined sample at 33°C (in red in Figures 2CD), and corresponding simulation snapshots at five selected time instants (as marked in Figures 2CD) are shown in Figure 2E. The





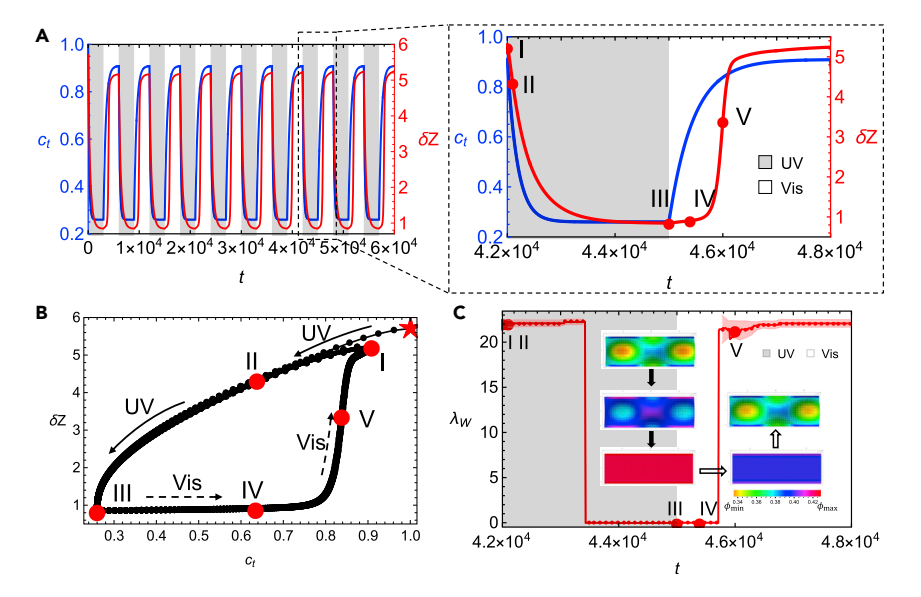


Figure 3. Dynamic restructuring of buckling patterns in the confined sample upon UV/Vis light cycles at 33 °C The switching time is $\Delta t = 3 \times 10^3$.

(A) Time evolution of the fraction of trans-Azo, c_t (blue, left axis) and the amplitude, δZ (red, right axis). The patterns are fully developed in the α -CD solution in the dark before introducing UV/Vis light cycles.

(B) The amplitude δZ as a function of c_t during all ten UV/Vis irradiation cycles. The starting point of the first cycle (t=0) is marked by the red star. The solid and dashed arrows indicate the UV and Vis light irradiation portions, respectively.

(C) Time evolution of the wavelength λ_W during a single cycle as highlighted in (A). The insets show partial top views of

(C) Time evolution of the wavelength λ_W during a single cycle as highlighted in (A). The insets show partial top views of morphologies in the middle of the sample at I-V time instances as marked in (A and B).

swelling ratio upon the equilibration of the free sample at 33°C is below the critical value α_c^* under UV irradiation (Figure 1C, green curve), and above this value under visible light (Figure 1C, blue curve). Hence, as anticipated based on these estimates, the patterns are erased during sufficiently prolonged exposure to UV irradiation at this temperature and are reformed upon visible light irradiation. Similar to the previous scenario, the wavelength remains approximately constant (at $\lambda_W = 21.5 \pm 0.21$) when the sample is buckled; larger standard deviations are observed when the patterns begin reforming near the center of the sample under visible light irradiation (snapshot IX in Figure 2E). The amplitude δZ gradually decreases under UV irradiation upon reaching the equilibrium value and increases under visible light (Figure 2D). To summarize, these results show that the pattern formation in hydrogels with host-guest interactions can be effectively controlled by applying UV and visible light irradiations.

Response under cyclic illumination

We next introduce ten UV/Vis irradiation cycles to the initially buckled sample immersed in the α -CD solution in the dark at 33°C as described above and probe the effect of the time of switching of irradiation on the cyclic response of the confined sample. We first focus on the case where UV and visible light irradiation times are alternated every $\Delta t = 3 \times 10^3$; sufficiently long irradiation times allow c_t to reach the equilibrium values, $\tilde{c}_t = 0.909$ (Vis) and 0.260 (UV) during each cycle (blue, left axis in Figure 3A). We illustrate the time evolution of patterns developed within a single equilibrated cycle (as marked in the inset in Figure 3A). Similar to the scenario above, these results show that the amplitude δZ of the sample gradually decreases and saturates to the value close to the thickness of the flat sample upon equilibration under UV irradiation (Figure 3B). Upon visible light irradiation, the sample remains flat and exhibits a slight increase in δZ at early times until small out-of-plane undulations appear close to its center, followed by a sharp increase and then a gradual increase of the amplitude at the end of the cycle. The wavelength (Figure 3C) remains approximately constant ($\lambda_W = 22.1 \pm 0.41$) as long as the sample is buckled, similar to the behavior observed in Figure 2C at the same temperature (red curve). Further, the positions of the peaks along the length of the buckled sample remain approximately constant (see the snapshots of the portions of the sample in Figure 3C), while the amplitude varies significantly. These observations indicate that the topography of the confined sample strongly depends on the illumination history. The parametric dependence of δZ on c_t for all ten cycles is provided in Figure 3B; the star



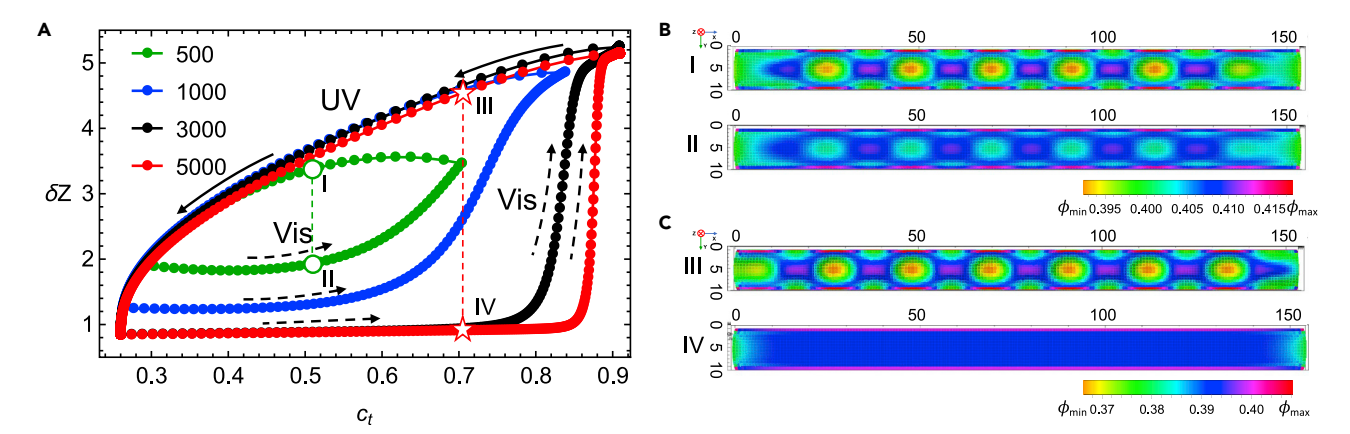


Figure 4. Effects of the switching time

(A) Amplitude as a function of c_t within an equilibrated cycle at 33°C for four switching times as listed in the legend. The portions of UV and visible light irradiation are indicated by solid and dashed arrows, respectively. The open circles correspond to the states at $c_t = 0.51$ during UV (I) and visible (II) light irradiation with $\Delta t = 500$. The open stars correspond to the states at $c_t = 0.7$ during UV (III) and visible (IV) light irradiation with $\Delta t = 5 \times 10^3$. (B and C) The top views of morphologies at time instances I-IV as marked in (A). The color represents the local φ according to the respective color bar.

marks the initial state (beginning of the first cycle) and solid and dashed arrows mark the UV and Vis portions of the light irradiation cycles. This figure illustrates that with the exception of the equilibration during the first cycle, the dynamics during the remaining cycles overlap, so that only the single equilibrated cycle can be used for further analysis later in discussion.

In the next series of simulations, we vary the duration of the application of UV/Vis light keeping the remaining parameters and initial conditions as introduced above; specifically, we choose $\Delta t = 500$, 1×10^3 , and 5×10^3 in addition to $\Delta t = 3 \times 10^3$ discussed above. We plot the dependence of the amplitude δZ and the wavelength λ_W on c_t for the single equilibrated cycle in Figures 4A and S5, respectively; the black curves in these plots correspond to the data discussed in Figure 3. In addition, the $\delta Z(c_t)$ and $\lambda_W(c_t)$ for all ten cycles at $\Delta t = 500$ and 3×10^3 are provided in Figure S6.

For the shorter switching times probed (green and blue curves in Figure 4), the equilibrium photostationary value $\tilde{c}_t = 0.260$ is no longer reached upon UV irradiation, thereby while the amplitude decreases significantly (solid arrows in Figure 4A), the patterns are not fully erased by UV irradiation and the wavelength remains approximately constant (Figure S6A). In these two scenarios, an application of visible light results in the gradual increase of the amplitude, with the clear hysteresis in $\delta Z(c_t)$ so that significantly lower amplitude is observed at the same c_t upon irradiation with visible light than that upon irradiation with UV (compare lower and upper portions of hysteresis loops in Figure 4 for blue and green curves, respectively, and representative images in Figure 4B). During the entire cycle, the samples in these two scenarios remain buckled with approximately constant wavelength (Figure S5), but with distinct variations in amplitude controlled by the illumination cycle.

On the contrary, for sufficiently long switching times (red and black curves in Figure 4A), the patterns are completely erased during the UV irradiation portion of the cycle. Correspondingly the sample remains flat during the visible irradiation portion of the illumination cycle until the stability is lost at sufficiently high values of c_t . The hysteresis loops become wider with an increase in Δt , with either buckled or flat morphology observed at a range of values of c_t for UV or visible irradiation portions of the cycle. An application of the same ten illumination cycles with $\Delta t = 3 \times 10^3$ at 20°C (Figure S7C) results in essentially an absence of hysteresis in systems' response to the changes in illumination. This is attributed to the fact that the effective swelling ratio significantly higher than the threshold (Figure 1C) enables the samples to remain buckled during all cycles for the tested values of switching time.

Prescribing soft boundaries using patterned illuminations

In the next series of simulations, we focus on triggering pattern formation and controlling characteristics of patterns formed in hydrogel films freely suspended in the α -CD solution by means of patterned UV light irradiation. The samples are initially flat and equilibrated in pure water in the dark in the absence of





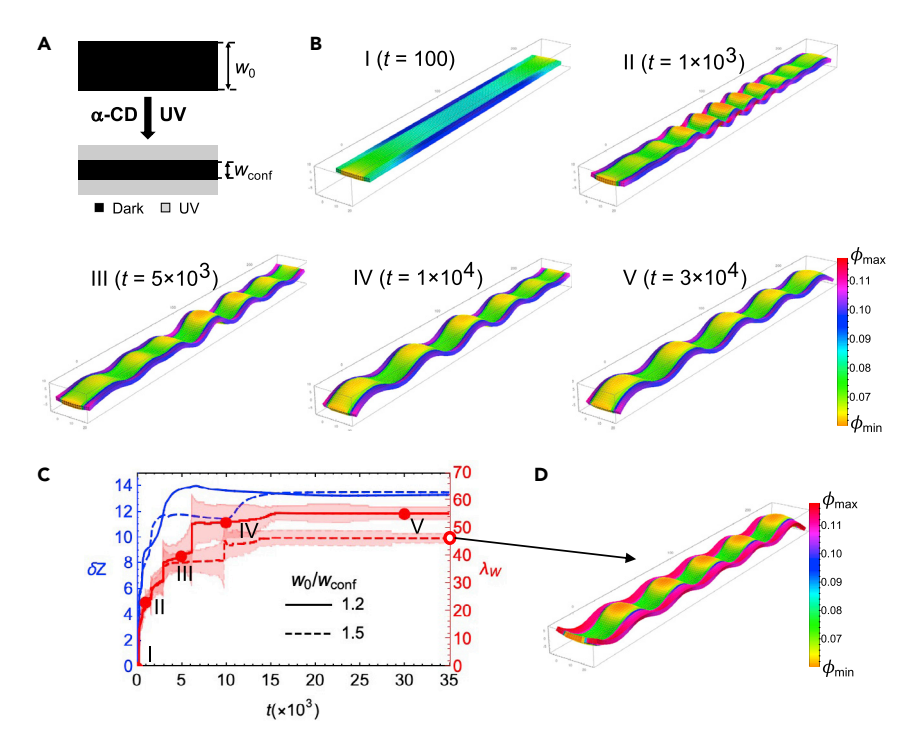


Figure 5. Pattern formation in free samples upon adding α -CD solution under the patterned UV irradiation at $20^{\circ}C$

- (A) Schematics of illumination pattern.
- (B) The snapshots of morphologies at five time instances (marked I \sim V in (C)).
- (C) Time evolution of the wavelength λ_W (blue, left axis) and the amplitude δZ (red, right axis) in sample with w_0/w_{conf} as listed in the legend. The free samples are initially equilibrated in pure water in the dark at 20°C.
- (D) The snapshot of the morphology of the free sample ($w_0/w_{conf} = 1.5$) at equilibrium under patterned illumination (as marked by the open circle in (C)). The color in (B) and (D) indicates the local φ according to the respective color bar.

confinements at 20° C. We then keep the middle portion of the sample (black region of width w_{conf} in the schematic in Figure 5A) in the dark and introduce UV irradiation over the remainder of the sample. It is assumed that the α -CD solution is added at the same time when the patterned UV irradiation is introduced. The width of the region kept in the dark is chosen equal to the initial width of the sample with both long edges fixed at 20° C as considered above (Figure 2B); specifically, we set $w_{conf} = 15.21$. The size of the sample in this series of simulations is chosen as $200 \times 18 \times 3$ nodes (dimensionless size of $216.23 \times 18.47 \times 2.17$ at 20° C) and $w_0/w_{conf} = 1.2$. The aim herein is to introduce localized shrinking along the long edges by means of UV irradiation, which in turn is expected to introduce soft confinement along the long edges and promote pattern formation in this system.

The snapshots of the morphology development under patterned illumination are provided in Figure 5B. The free sample initially swells along all three directions and remains flat at early times upon the addition of the α -CD units. The swelling is clearly restricted within the regions under UV illumination (gray regions in Figure 5A and dark blue regions indicating higher polymer volume fraction in snapshot I in Figure 5B). Thereby two relatively shrunk stripes along both sides constrain the swelling of the middle portion of the sample, acting as an effective soft confinement. Sufficiently high compression exerted by these illuminated regions triggers mechanical instability, with the undulations appearing in the center of the sample and propagating toward both ends (snapshots II and III in Figure 5B). Relatively smaller undulations observed during early times evolve (snapshot IV in Figure 5B) and develop into regular buckling patterns at equilibrium (snapshot V in Figure 5B). No in-plane (x-y plane) rotation or translation of the entire sample was observed. To characterize the buckling patterns formed, we focus on the middle portion of the sample and adapt the characterizations defined above. The time evolution of the amplitude δZ (in blue, left axis) and wavelength λ_W (in red, right axis) during the pattern formation in the scenario depicted in Figure 5B (solid lines) are both shown in Figure 5C. Comparison between these characteristics and corresponding characteristics of the sample with rigid confinement along both edges immersed in the α -CD solution





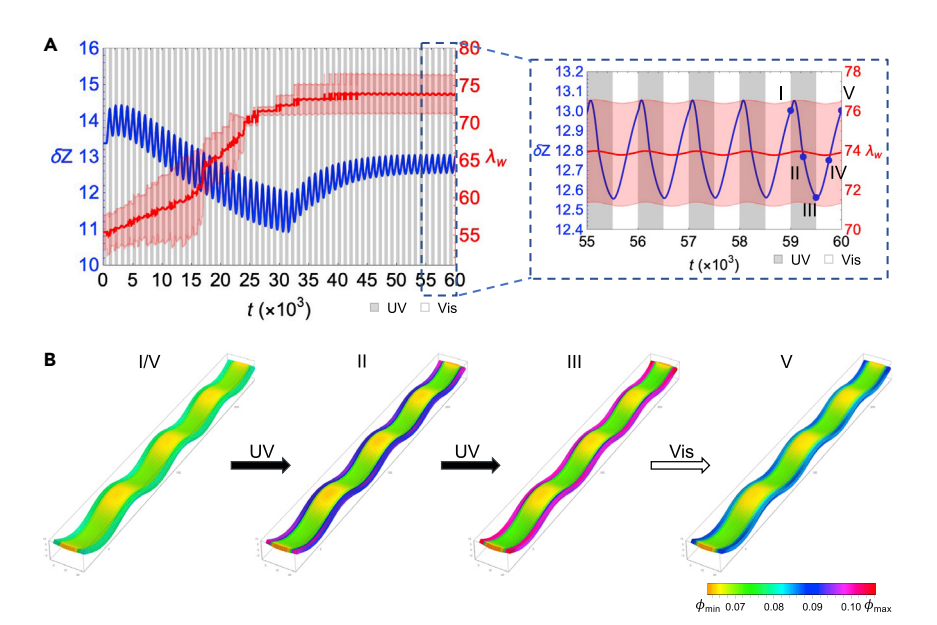


Figure 6. Dynamic restructuring of buckling patterns in the free sample upon patterned UV/Vis irradiation cycles at 20 °C

The switching time is $\Delta t = 500$.

(A) Time evolution of the amplitude, δZ (blue, left axis), and the wavelength, λ_W (red, right axis). The buckling patterns are fully developed in α -CD solution under patterned UV irradiation before introducing UV/Vis light cycles. The inset (right) is the zoomed image of the highlighted region as marked.

(B) The snapshots of morphologies at I-V time instances as marked in the inset in (A). The color indicates the local φ according to the color bar.

(black curves in Figures S4AB and morphology snapshot in Figure S4D) shows nearly 2-fold increase in the wavelength for the case of soft confinement.

To probe the effect of the width of the illuminated region which effectively introduces the soft confinement, we kept all the parameters and illumination conditions fixed but chose the wider sample (initial sample size is $216.23 \times 22.82 \times 2.17$) in the next simulation scenario. Specifically, we kept the width of the region in the dark, w_{conf} , fixed, so that the same illumination pattern results in significant increase of the width of the soft confinement region prescribed by the illumination ($w_0/w_{\text{conf}}=1.5$). Our results show that an increase in the w_0/w_{conf} ratio results in a significant decrease of the wavelength upon equilibration but the amplitude δZ remains approximately the same (see dashed curves in Figure 5C). The snapshot of the buckling pattern in the wider sample ($w_0/w_{\text{conf}}=1.5$) in equilibrium is provided in Figure 5D.

In the next series of simulations, we apply patterned UV/Vis irradiation cycles to the equilibrated sample (snapshot V in Figure 5B) to dynamically control pattern formation via remotely prescribed soft confinements. The middle region remains in the dark and two striped regions on both sides are illuminated by alternating UV and Vis irradiation, the temperature is held constant at 20°C. We probe the switching time of $\Delta t = 500$ and run the simulation for $t = 6 \times 10^4$ (corresponding to 3.33 h). We track the time evolutions of the amplitude, δZ (in blue, right axis in Figure 6A), and the wavelength, λ_W (in red, right axis). Our results show that the sample remains buckled during the entire simulation. Note that a significantly longer time is required for the sample to achieve an equilibrated cycle than for the case of the sample with both long edges clamped. An increase in the wavelength λ_W over multiple cycles (Figure 6A, red curve) indicates gradual restructuring of patterns with a corresponding decrease in the number of wavelengths that fit within the sample length. The evolution of δZ and λ_W during an equilibrated cycle is highlighted in the inset in Figure 6A, and the representative snapshots are provided in Figure 6B. The parametric plot of $\delta Z(\langle c_t \rangle)$ during an equilibrated cycle (Figure S8) shows that in response to UV and Vis light the patterns are restructured primarily via the variation in the amplitude. Similar trends are also observed during the cyclic illumination of the same sample with a longer switching time of $\Delta t = 3 \times 10^3$ (Figure S9) and upon the cyclic illumination of the wider sample ($w_0/w_{conf} = 1.5$) (Figure S10).

Article



DISCUSSION

We developed a computational model capturing the dynamics of hydrogels with host-guest interactions. Specifically, we focused on PNIPPAm hydrogels with pendant azobenzene groups immersed into the α -CD solution. The proposed model extends the three-dimensional gLSM approach and is validated with respect to the available experimental results. Using the developed model, we characterized the dynamics of hydrogels with host-guest interactions in the dark, under uniform UV and visible irradiation including cyclic irradiation, and under well-defined patterned illumination. We demonstrated that simply placing the samples constrained along their long edges in the dark into the α -CD solution results in swelling-induced instabilities and subsequent formation of regular buckling patterns upon equilibration. While swelling is caused by the formation of complexes in which trans-azobenzene moieties are accommodated by the α -CD cavities, an exposure to UV irradiation drives the trans-to-cis isomerization and dissociation of these complexes, leading to hydrogel deswelling. Hence the variations in illumination conditions introduce simple and robust means to control pattern formation and restructuring in thin hydrogel films under rigid and soft confinements and to regulate hysteresis loops in response to cyclic illumination. The soft confinements are introduced dynamically via illuminating specific regions of thin samples with UV light so that the regions of higher rigidity are introduced. Our results demonstrate that onset of buckling and features of patterns formed along with hysteresis in the systems' response can be effectively controlled in hydrogels with hostguest interactions via well-defined illumination patterns. Photocontrol of pattern formation is of particular interest since illumination introduces remote and non-invasive means to induce, erase, and rewrite patterns required for imparting specific functionalities in soft hydrogel-based materials. Further, designing synthetic hydrogels with controlled hysteresis loops is an important step toward introducing robust feedback mechanisms in soft functional materials.

Limitations of the study

This computational study focuses on modeling the dynamics of thin hydrogels with photo-responsive host-guest interactions. Introducing light attenuation through the thickness of the sample can extend the proposed model to consider significantly thicker samples, which in turn could benefit the investigation of patterns formed due to the swelling gradient in the thickness direction. Further, the proposed approach considers Neo-Hookean elasticity of polymer matrix and does not account for any possible effects of viscoelasticity.

STAR*METHODS

Detailed methods are provided in the online version of this paper and include the following:

- KEY RESOURCES TABLE
- RESOURCE AVAILABILITY
 - Lead contact
 - O Materials availability
 - O Data and code availability
- METHOD DETAILS
 - Computational methods
 - O Estimating the Poisson's ratio of the azobenzene-functionalized hydrogels

SUPPLEMENTAL INFORMATION

Supplemental information can be found online at https://doi.org/10.1016/j.isci.2022.105606.

ACKNOWLEDGMENTS

This work was supported in part by the National Science Foundation EPSCoR Program under NSF Award No. OIA-1655740. Any opinions, findings and conclusions or recommendations expressed in this material are those of the author(s) and do not necessarily reflect those of the National Science Foundation. Clemson University is acknowledged for the generous allotment of compute time on Palmetto cluster.

AUTHOR CONTRIBUTIONS

O.K. and Y.X. contributed to conceptualization; Y.X. and O.K. contributed to model development and validation, Y.X. generated the simulations data, performed initial data analysis, visualization, and data





curation, Y.X. and O.K. performed formal analysis and investigation, Y.X. wrote original draft, Y.X. and O.K. edited article, O.K. supervised all the aspects of the work.

DECLARATION OF INTERESTS

The authors declare no competing interests.

Received: August 8, 2022 Revised: November 1, 2022 Accepted: November 12, 2022 Published: December 22, 2022

REFERENCES

- Yewdall, N.A., Mason, A.F., and van Hest, J.C.M. (2018). The hallmarks of living systems: towards creating artificial cells. Interface Focus 8, 20180023. https://doi.org/10.1098/ rsfs.2018.0023.
- Newman, S.A., and Comper, W.D. (1990). 'Generic' physical mechanisms of morphogenesis and pattern formation. Development 110, 1–18. https://doi.org/10. 1242/dev.110.1.1.
- Rosales, A.M., and Anseth, K.S. (2016). The design of reversible hydrogels to capture extracellular matrix dynamics. Nat. Rev. Mater. 1, 15012. https://doi.org/10.1038/ natrevmats.2015.12.
- Tokudome, Y., Kuniwaki, H., Suzuki, K., Carboni, D., Poologasundarampillai, G., and Takahashi, M. (2016). Thermoresponsive wrinkles on hydrogels for soft actuators. Adv. Mater. Interfac. 3, 1500802. https://doi.org/ 10.1002/admi.201500802.
- Guvendiren, M., Burdick, J.A., and Yang, S. (2010). Solvent induced transition from wrinkles to creases in thin film gels with depth-wise crosslinking gradients. Soft Matter 6, 5795–5801. https://doi.org/10. 1039/c0sm00317d.
- Chan, H.F., Zhao, R., Parada, G.A., Meng, H., Leong, K.W., Griffith, L.G., and Zhao, X. (2018). Folding artificial mucosa with cellladen hydrogels guided by mechanics models. Proc. Natl. Acad. Sci. USA 115, 7503– 7508. https://doi.org/10.1073/pnas. 1802361115.
- Mora, T., and Boudaoud, A. (2006). Buckling of swelling gels. Eur. Phys. J. E Soft Matter 20, 119–124. https://doi.org/10.1140/epje/i2005-10124-5.
- DuPont Jr, S.J., Cates, R.S., Stroot, P.G., and Toomey, R. (2010). Swelling-induced instabilities in microscale, surface-confined poly(N-isopropylacryamide) hydrogels. Soft Matter 6, 3876–3882. https://doi.org/10. 1039/c0sm00021c.
- Xiong, Y., and Kuksenok, O. (2021). Mechanical adaptability of patterns in constrained hydrogel membranes. Langmuir 37, 4900–4912. https://doi.org/10.1021/acs. langmuir.1c00138.
- Dervaux, J., and Amar, M.B. (2012).
 Mechanical instabilities of gels. Annu. Rev.

- Condens. Matter Phys. 3, 311–332. https://doi.org/10.1146/annurev-conmatphys-062910-140436.
- Wen, X., Sun, S., and Wu, P. (2020). Dynamic wrinkling of a hydrogel-elastomer hybrid microtube enables blood vessel-like hydraulic pressure sensing and flow regulation. Mater. Horiz. 7, 2150–2157. https://doi.org/10.1039/d0mh00089b.
- Guvendiren, M., Burdick, J.A., and Yang, S. (2010). Kinetic study of swelling-induced surface pattern formation and ordering in hydrogel films with depth-wise crosslinking gradient. Soft Matter 6, 2044–2049. https:// doi.org/10.1039/b927374c.
- Guvendiren, M., Yang, S., and Burdick, J.A. (2009). Swelling-induced surface patterns in hydrogels with gradient crosslinking density. Adv. Funct. Mater. 19, 3038–3045. https://doi. org/10.1002/adfm.200900622.
- Wu, Z., Bouklas, N., and Huang, R. (2013). Swell-induced surface instability of hydrogel layers with material properties varying in thickness direction. Int. J. Solid Struct. 50, 578–587. https://doi.org/10.1016/j.ijsolstr. 2012.10.022.
- Lei, X., Ye, D., Chen, J., Tang, S., Sun, P., Chen, L., Lu, A., Du, Y., and Zhang, L. (2019). Customizable multidimensional selfwrinkling structure constructed via modulus gradient in chitosan hydrogels. Chem. Mater. 31, 10032–10039. https://doi.org/10.1021/ acs.chemmater.9b02812.
- Wu, Z.L., Moshe, M., Greener, J., Therien-Aubin, H., Nie, Z., Sharon, E., and Kumacheva, E. (2013). Three-dimensional shape transformations of hydrogel sheets induced by small-scale modulation of internal stresses. Nat. Commun. 4, 1586. https://doi. org/10.1038/ncomms2549.
- Jeon, S.J., Hauser, A.W., and Hayward, R.C. (2017). Shape-morphing materials from stimuli-responsive hydrogel hybrids. Acc. Chem. Res. 50, 161–169. https://doi.org/10. 1021/acs.accounts.6b00570.
- Kuenstler, A.S., Lahikainen, M., Zhou, H., Xu, W., Priimagi, A., and Hayward, R.C. (2020). Reconfiguring Gaussian curvature of hydrogel sheets with photoswitchable hostguest interactions. ACS Macro Lett. 9, 1172– 1177. https://doi.org/10.1021/acsmacrolett. 0c00469.

- Rau, H. (2002). 1 photoisomerization of azobenzenes. In Photoreactive Organic Thin Films, Z. Sekkat and W. Knoll, eds. (Academic Press), pp. 3–47. https://doi.org/10.1016/ B978-012635490-4/50002-0.
- Wang, L., and Li, Q. (2018). Photochromism into nanosystems: towards lighting up the future nanoworld. Chem. Soc. Rev. 47, 1044– 1097. https://doi.org/10.1039/c7cs00630f.
- Bandara, H.M.D., and Burdette, S.C. (2012). Photoisomerization in different classes of azobenzene. Chem. Soc. Rev. 41, 1809–1825. https://doi.org/10.1039/c1cs15179g.
- Kumar, G.S., and Neckers, D.C. (1989). Photochemistry of azobenzene-containing polymers. Chem. Rev. 89, 1915–1925. https:// doi.org/10.1021/cr00098a012.
- Matsubara, K., Watanabe, M., and Takeoka, Y. (2007). A thermally adjustable multicolor photochromic hydrogel. Angew. Chem. Int. Ed. Engl. 46, 1688–1692. https://doi.org/10. 1002/anie.200603554.
- Irie, M. (1993). Stimuli-responsive poly(N-isopropylacrylamide) photoinduced and chemical-induced phase-transitions. Adv. Polym. Sci. 110, 49–65. https://doi.org/10.1007/RFh0021128
- Kang, M.S., and Gupta, V.K. (2002). Photochromic cross-links in thermoresponsive hydrogels of poly(Nisopropylacrylamide): enthalpic and entropic consequences on swelling behavior. J. Phys. Chem. B 106, 4127–4132. https://doi.org/10. 1021/jp014027w.
- Hu, Q.D., Tang, G.P., and Chu, P.K. (2014). Cyclodextrin-based host-guest supramolecular nanoparticles for delivery: from design to applications. Acc. Chem. Res. 47, 2017–2025. https://doi.org/10.1021/ ar500055s
- Zhang, Y.M., Liu, Y.H., and Liu, Y. (2020). Cyclodextrin-based multistimuli-responsive supramolecular assemblies and their biological functions. Adv. Mater. 32, e1806158. https://doi.org/10.1002/adma. 201806158.
- Yan, X., Wang, F., Zheng, B., and Huang, F. (2012). Stimuli-responsive supramolecular polymeric materials. Chem. Soc. Rev. 41, 6042–6065. https://doi.org/10.1039/ c2cs35091b.

Article



- Qu, D.H., Wang, Q.C., Zhang, Q.W., Ma, X., and Tian, H. (2015). Photoresponsive hostguest functional systems. Chem. Rev. 115, 7543–7588. https://doi.org/10.1021/ cr5006342.
- Zhu, L., Zhao, C., Zhang, J., and Gong, D. (2015). Photocontrollable volume phase transition of an azobenzene functionalized microgel and its supramolecular complex. RSC Adv. 5, 84263–84268. https://doi.org/10. 1039/c5ra15256a.
- Takashima, Y., Hatanaka, S., Otsubo, M., Nakahata, M., Kakuta, T., Hashidzume, A., Yamaguchi, H., and Harada, A. (2012). Expansion-contraction of photoresponsive artificial muscle regulated by host-guest interactions. Nat. Commun. 3, 1270. https:// doi.org/10.1038/ncomms2280.
- Zheng, Z., Hu, J., Wang, H., Huang, J., Yu, Y., Zhang, Q., and Cheng, Y. (2017). Dynamic softening or stiffening a supramolecular hydrogel by ultraviolet or near-infrared light. ACS Appl. Mater. Interfaces 9, 24511–24517. https://doi.org/10.1021/acsami.7b07204.
- Kuksenok, O., Yashin, V.V., and Balazs, A.C. (2008). Three-dimensional model for chemoresponsive polymer gels undergoing the Belousov-Zhabotinsky reaction. Phys. Rev. E Stat. Nonlin. Soft Matter Phys. 78, 041406. https://doi.org/10.1103/PhysRevE. 78.041406
- Toh, W., Ding, Z., Yong Ng, T., and Liu, Z. (2015). Wrinkling of a polymeric gel during transient swelling. J. Appl. Mech. 82. https:// doi.org/10.1115/1.4030327.
- Liu, Z.S., Swaddiwudhipong, S., Cui, F.S., Hong, W., Suo, Z., and Zhang, Y.W. (2011). Analytical solutions of polymeric gel structures under buckling and wrinkle. Int. J. Appl. Mech. 03, 235–257. https://doi.org/10. 1142/S1758825111000968.
- Li, B., Cao, Y.P., Feng, X.Q., and Gao, H. (2012). Mechanics of morphological instabilities and surface wrinkling in soft materials: a review. Soft Matter 8, 5728–5745. https://doi.org/10.1039/C2SM00011C.
- Chen, D., Yoon, J., Chandra, D., Crosby, A.J., and Hayward, R.C. (2014). Stimuli-responsive buckling mechanics of polymer films.
 J. Polym. Sci. Part B Polym. Phys. 52, 1441– 1461. https://doi.org/10.1002/polb.23590.
- Rodríguez-Hernández, J. (2015). Wrinkled interfaces: taking advantage of surface instabilities to pattern polymer surfaces. Prog. Polym. Sci. 42, 1–41. https://doi.org/10. 1016/j.progpolymsci.2014.07.008.
- Yashin, V.V., and Balazs, A.C. (2006). Pattern formation and shape changes in selfoscillating polymer gels. Science 314, 798–801. https://doi.org/10.1126/science. 1132412.
- Yashin, V.V., and Balazs, A.C. (2007). Theoretical and computational modeling of self-oscillating polymer gels. J. Chem. Phys. 126, 124707. https://doi.org/10.1063/1. 26772951.

- Yoshida, R., Tanaka, M., Onodera, S., Yamaguchi, T., and Kokufuta, E. (2000). Inphase synchronization of chemical and mechanical oscillations in self-oscillating gels. J. Phys. Chem. A 104, 7549–7555. https://doi. org/10.1021/jp0011600.
- Chen, I.C., Kuksenok, O., Yashin, V.V., Moslin, R.M., Balazs, A.C., and Van Vliet, K.J. (2011). Shape- and size-dependent patterns in selfoscillating polymer gels. Soft Matter 7, 3141– 3146. https://doi.org/10.1039/COSM01007C.
- 43. Kuksenok, O., Yashin, V.V., Kinoshita, M., Sakai, T., Yoshida, R., and Balazs, A.C. (2011). Exploiting gradients in cross-link density to control the bending and self-propelled motion of active gels. J. Mater. Chem. 21, 8360–8371. https://doi.org/10.1039/c0jm03426f.
- Yuan, P., Kuksenok, O., Gross, D.E., Balazs, A.C., Moore, J.S., and Nuzzo, R.G. (2013). UV patternable thin film chemistry for shape and functionally versatile self-oscillating gels. Soft Matter 9, 1231–1243. https://doi.org/10. 1039/C2SM27100A.
- Yashin, V.V., Kuksenok, O., and Balazs, A.C. (2010). Modeling autonomously oscillating chemo-responsive gels. Prog. Polym. Sci. 35, 155–173. https://doi.org/10.1016/j. progpolymsci.2009.10.003.
- Kuksenok, O., Dayal, P., Bhattacharya, A., Yashin, V.V., Deb, D., Chen, I.C., Van Vliet, K.J., and Balazs, A.C. (2013). Chemoresponsive, self-oscillating gels that undergo biomimetic communication. Chem. Soc. Rev. 42, 7257–7277. https://doi.org/10.1039/ c3c35407k
- 47. Yashin, V.V., Suzuki, S., Yoshida, R., and Balazs, A.C. (2012). Controlling the dynamic behavior of heterogeneous self-oscillating gels. J. Mater. Chem. 22, 13625–13636. https://doi.org/10.1039/c2jm32065g.
- Dayal, P., Kuksenok, O., and Balazs, A.C. (2009). Using light to guide the self-sustained motion of active gels. Langmuir 25, 4298– 4301. https://doi.org/10.1021/la900051b.
- Dayal, P., Kuksenok, O., Bhattacharya, A., and Balazs, A.C. (2012). Chemically-mediated communication in self-oscillating, biomimetic cilia. J. Mater. Chem. 22, 241–250. https://doi. org/10.1039/c1jm13787e.
- Dayal, P., Kuksenok, O., and Balazs, A.C. (2013). Reconfigurable assemblies of active, autochemotactic gels. Proc. Natl. Acad. Sci. USA 110, 431–436. https://doi.org/10.1073/ pnas.1213432110.
- Kuksenok, O., Deb, D., Dayal, P., and Balazs, A.C. (2014). Modeling chemoresponsive polymer gels. Annu. Rev. Chem. Biomol. Eng. 5, 35–54. https://doi.org/10.1146/annurevchembioeng-060713-035949.
- Dayal, P., Kuksenok, O., and Balazs, A.C. (2014). Directing the behavior of active, self-oscillating gels with light. Macromolecules 47, 3231–3242. https://doi.org/10.1021/ ma402430b.
- 53. Ren, L., Yuan, L., Gao, Q., Teng, R., Wang, J., and Epstein, I.R. (2020). Chemomechanical

- origin of directed locomotion driven by internal chemical signals. Sci. Adv. 6, 9125. https://doi.org/10.1126/sciadv.aaz9125.
- Ren, L., She, W., Gao, Q., Pan, C., Ji, C., and Epstein, I.R. (2016). Retrograde and direct wave locomotion in a photosensitive selfoscillating gel. Angew. Chem. Int. Ed. Engl. 55, 14301–14305. https://doi.org/10.1002/ anie.201608367.
- Kuksenok, O., and Balazs, A.C. (2013). Modeling the photoinduced reconfiguration and directed motion of polymer gels. Adv. Funct. Mater. 23, 4601–4610. https://doi.org/ 10.1002/adfm.201203876.
- Kuksenok, O., and Balazs, A.C. (2015). Designing dual-functionalized gels for self-reconfiguration and autonomous motion. Sci. Rep. 5, 9569. https://doi.org/10.1038/ srep09569.
- Bortolus, P., and Monti, S. (1987). Cis reversible trans photoisomerization of azobenzene cyclodextrin inclusion complexes. J. Phys. Chem. A 91, 5046–5050. https://doi.org/10.1021/j100303a032.
- Tamesue, S., Takashima, Y., Yamaguchi, H., Shinkai, S., and Harada, A. (2010). Photoswitchable supramolecular hydrogels formed by cyclodextrins and azobenzene polymers. Angew. Chem. Int. Ed. Engl. 49, 7461–7464. https://doi.org/10.1002/anie. 201003567.
- Wang, Y., Ma, N., Wang, Z., and Zhang, X. (2007). Photocontrolled reversible supramolecular assemblies of an azobenzene-containing surfactant with alpha-cyclodextrin. Angew. Chem. Int. Ed. Engl. 46, 2823–2826. https://doi.org/10.1002/ania.2006.04882
- Royes, J., Courtine, C., Lorenzo, C., Lauth-de Viguerie, N., Mingotaud, A.F., and Pimienta, V. (2020). Quantitative kinetic modeling in photoresponsive supramolecular chemistry: the case of water-soluble azobenzene/ cyclodextrin complexes. J. Org. Chem. 85, 6509–6518. https://doi.org/10.1021/acs.joc. 0c00461.
- Zimmerman, G., Chow, L.Y., and Paik, U.J. (1958). The photochemical isomerization of azobenzene. J. Am. Chem. Soc. 80, 3528– 3531. https://doi.org/10.1021/ja01547a010.
- Mechau, N., Saphiannikova, M., and Neher, D. (2005). Dielectric and mechanical properties of azobenzene polymer layers under visible and ultraviolet irradiation. Macromolecules 38, 3894–3902. https://doi. org/10.1021/ma0479316.
- Serra, F., and Terentjev, E.M. (2008). Effects of solvent viscosity and polarity on the isomerization of azobenzene. Macromolecules 41, 981–986. https://doi. org/10.1021/ma702033e.
- 64. Parker, R.M., Wales, D.J., Gates, J.C., Smith, P.G.R., and Grossel, M.C. (2016). Tracking a photo-switchable surface-localised supramolecular interaction via refractive index. J. Mater. Chem. C 4, 1178–1185. https://doi.org/10.1039/c5tc03774c.





- **65.** Hill, T.L. (1960). An Introduction to Statistical Thermodynamics (Addison-Weley).
- Atkin, R.J., and Fox, N. (1980). An Introduction to the Theory of Elasticity (Dover Publications).
- 67. Mark, J.E., and Erman, B. (2007). Rubberlike Elasticity: A Molecular Primer, Second edition (Cambridge University Press).
- Hirotsu, S. (1991). Softening of bulk modulus and negative Poisson ratio near the volume phase-transition of polymer gels. J. Chem. Phys. 94, 3949–3957. https://doi.org/10.1063/ 1460677
- Lopez, C.G., and Richtering, W. (2017). Does Flory-Rehner theory quantitatively describe the swelling of thermoresponsive microgels? Soft Matter 13, 8271–8280. https://doi.org/ 10.1039/c7sm01274h.
- Wolfram Research, Inc (2021). Mathematica, Version 12, Third edition (Wolfram Research, Inc).
- Phua, D.I., Herman, K., Balaceanu, A., Zakrevski, J., and Pich, A. (2016). Reversible size modulation of aqueous microgels via orthogonal or combined application of thermo- and phototriggers. Langmuir 32, 3867–3879. https://doi.org/10.1021/acs. langmuir.6b00241.
- Beharry, A.A., and Woolley, G.A. (2011). Azobenzene photoswitches for biomolecules. Chem. Soc. Rev. 40, 4422– 4437. https://doi.org/10.1039/c1cs15023e.
- Yang, Y.Z., Tang, Q., Gong, C.B., Ma, X.B., Peng, J.D., and Lam, M.H.W. (2014). Ultrasensitive detection of bisphenol A in aqueous media using photoresponsive surface molecular imprinting polymer microspheres. New J. Chem. 38, 1780–1788. https://doi.org/10.1039/c3nj015981.
- Xu, X., Zhou, N., Zhu, J., Tu, Y., Zhang, Z., Cheng, Z., and Zhu, X. (2010). The first example of main-chain cyclic azobenzene polymers. Macromol. Rapid Commun. 31, 1791–1797. https://doi.org/10.1002/marc. 201000218.

- Li, L., Lu, B., Zhang, Y., Xing, X., Wu, X., and Liu, Z. (2015). Multi-sensitive copolymer hydrogels of N-isopropylacrylamide with several polymerizable azobenzenecontaining monomers. J. Polym. Res. 22, 176. https://doi.org/10.1007/s10965-015-0787-2.
- Hou, C., Zhou, C., and Cheng, J. (2021). Norbornenyl-based amphiphilic ABAtriblock azobenzene copolymers: synthesis, photoresponsive and self-assembly properties. Polymer 213, 123310. https://doi. org/10.1016/j.polymer.2020.123310.
- Wang, W., and Wang, M.Z. (2007). Effect of alpha-cyclodextrin on the photoisomerization of azobenzene functionalized hydroxypropyl methylcellulose in aqueous solution. Polym. Bull. 59, 537–544. https://doi.org/10.1007/s00289-007-0789-2.
- Liu, L., Li, N., Chen, M., Yang, H., Tang, Q., and Gong, C. (2018). Visible-light-responsive surface molecularly imprinted polymer for acyclovir through chicken skin tissue. ACS Appl. Bio Mater. 1, 845–852. https://doi.org/ 10.1021/acsabm.8b00275.
- Kanbara, T., Oshima, M., Imayasu, T., and Hasegawa, K. (1998). Preparation of new polymers containing an azobenzene group in the side chain by palladium-catalyzed polymer reaction and polycondensation and characterization of the polymers. Macromolecules 31, 8725–8730. https://doi. org/10.1021/ma981085f.
- Song, W., Qu, X., Li, Y., Li, J., Wang, C., and Ding, L. (2021). Azobenzene-containing alternating and random metathesis copolymers toward gaining more insight into photoisomerization properties. Macromolecules 54, 9185–9194. https://doi. org/10.1021/acs.macromol.0c02621.
- Paiva, G.M.S., Duarte, L.G.T.A., Faleiros, M.M., Atvars, T.D.Z., and Felisberti, M.I. (2020). Z-E isomerization of azobenzene based amphiphilic polyfurethane-urea)s: influence on the dynamic mechanical properties and the effect of the self-assembly in solution on the isomerization kinetics. Eur. Polym. J. 127, 109583. https://doi.org/10. 1016/j.eurpolymj.2020.109583.

- Eisenbach, C.D. (1978). Effect of polymer matrix on cis-trans isomerization of azobenzene residues in bulk polymers. Makromol. Chem. 179, 2489–2506. https:// doi.org/10.1002/macp.1978.021791014.
- Imai, Y., Naka, K., and Chujo, Y. (1999). Isomerization behavior of azobenzene chromophores attached to the side chain of organic polymer in organic-inorganic polymer hybrids. Macromolecules 32, 1013– 1017. https://doi.org/10.1021/ma981360y.
- Yogitha, S.N., Kumar, B., Raghavendra, I., Gupta, S.K., and Gupta, S.K. (2021). Effect of local electric field on trans to cis photoisomerization of azobenzene containing polymer. Mater. Sci. Eng. B 267, 115094. https://doi.org/10.1016/j.mseb.2021.115094.
- Rosales, A.M., Mabry, K.M., Nehls, E.M., and Anseth, K.S. (2015). Photoresponsive elastic properties of azobenzene-containing poly(ethylene-glycol)-based hydrogels. Biomacromolecules 16, 798–806. https://doi. org/10.1021/bm501710e.
- Homma, K., Chang, A.C., Yamamoto, S., Tamate, R., Ueki, T., and Nakanishi, J. (2021). Design of azobenzene-bearing hydrogel with photoswitchable mechanics driven by photoinduced phase transition for in vitro disease modeling. Acta Biomater. 132, 103–113. https://doi.org/10.1016/j.actbio.2021.03.028.
- Hirose, H., and Shibayama, M. (1998). Kinetics of volume phase transition in poly(Nisopropylacrylamide-co-acrylic acid) gels. Macromolecules 31, 5336–5342. https://doi. org/10.1021/ma980405s.
- 88. Doi, M. (2013). Soft Matter Physics (Oxford University Press).
- 89. Rubinstein, M., and Colby, R.H. (2003). Polymer Physics (Oxford University Press).
- Treloar, L.R.G. (2005). The Physics of Rubber Elasticity, Third edition (Oxford University Press).





STAR*METHODS

KEY RESOURCES TABLE

REAGENT or RESOURCE	SOURCE	IDENTIFIER			
Software and algorithms					
Wolfram Mathematica	Wolfram Research, Inc	https://www.wolfram.com/mathematica/			
Modified 3D gLSM	This paper; Zenodo	https://doi.org/10.5281/zenodo.7306921			

RESOURCE AVAILABILITY

Lead contact

Further information and requests for resources and reagents should be directed to and will be fulfilled by the lead contact, Olga Kuksenøk (okuksen@clemson.edu).

Materials availability

This study did not generate new unique reagents.

Data and code availability

- All data reported in this paper will be shared by the lead contact upon request.
- All original code has been deposited at Zenodo and is publicly available as of the date of publication.
 DOIs are listed in the key resources table.
- Any additional information required to reanalyze the data reported in this paper is available from the lead contact upon request.

METHOD DETAILS

Computational methods

We adapt three-dimensional gel Lattice Spring Model (3D gLSM) 33,45 to capture the dynamics of the azobenzene-functionalized PNIPAAm hydrogels immersed into the α -CD solution under UV irradiation and under the visible light; later in discussion we briefly introduce this methodology; more details can be found in the original publications. 33,45

Within the framework of gLSM, 40 the total energy of the deformed polymer network encompasses mixing energy U_{FH} (see Equation 2 above) and elastic energy contributions 67

$$U_{\rm el} = \frac{c_0}{2} \left(I_1 - 3 - \ln I_3^{1/2} \right)$$
 (Equation 7)

where $c_0 = \nu V_s/N_A$ is dimensionless crosslink density, ν is the density of polymer strands per unit volume at preparation, V_s is the molar volume of solvent, N_A is Avogadro constant, and $I_1 = \operatorname{tr} \widehat{\mathbf{B}}$. The dimensionless stress tensor is written as ${}^{39,40} \widehat{\boldsymbol{\sigma}} = -P(\varphi,c_t,T)\widehat{\mathbf{I}} + c_0 \frac{\varphi}{\varphi_0} \widehat{\mathbf{B}}$, where $\widehat{\mathbf{I}}$ is the unit tensor, φ_0 is the polymer volume fraction at preparation, and the isotropic pressure reads:

$$P(\varphi, c_{t}, T) = -\left[\varphi + \ln(1 - \varphi) + \chi(\varphi, T)\varphi^{2}\right] + c_{0}\frac{\varphi}{2\varphi_{0}} + \beta_{1}(1 - c_{t})\varphi + \beta_{2}c_{t}\varphi$$
 (Equation 8)

The last two terms in Equation 8 represent respective contributions from the free energy terms introduced in Equation 4, and $\chi(\varphi, T)$ is provided further later in discussion.

The reaction kinetics (Equation 2) is coupled with the gel elastodynamics³³ via the last two contributions in the isotropic pressure in Equation 8; the value of c_t is calculated herein from Equation 2. Within the 3D gLSM framework, an undeformed sample is represented by $(L_x - 1) \times (L_y - 1) \times (L_z - 1)$ cubic elements, where L_i is the number of nodes in the *i*-direction (i = x, y, z) as defined in ref.³³; the reference sample size chosen in our simulations is $200 \times 15 \times 3$ nodes unless specified otherwise. The forces acting on each node comprise elastic spring-like contributions from the next-nearest and next-next-nearest neighboring nodes and contributions from the isotropic pressure acting perpendicular to the respective faces of the





deformed element.³³ Hence, an increase in the volume fraction of the *cis*-Azo moieties, $(1-c_t)$, results in the isotropic pressure contribution proportional to β_1 (Equation 8), leading to the gel swelling. In a similar manner, an increase in the volume fraction of the *trans* – Azo in the presence of the α -CD units results in additional isotropic pressure contribution proportional to β_2 (Equation 8), leading to a distinct swelling as shown in the results section.

Estimating the Poisson's ratio of the azobenzene-functionalized hydrogels

The Poisson's ratio can be calculated as⁸⁸

$$v = \frac{(3K - 2G)}{2(3K + G)}$$
 (Equation 9)

where K and G are bulk and shear moduli. Based on our proposed model, the bulk and shear moduli of the azobenzene-functionalized PNIPAAm gel at a given temperature can be estimated as $^{68,88-90}$:

$$K = \varphi \frac{\partial \hat{\sigma}}{\partial \varphi} = \left[\frac{\varphi_{\text{eq}}^{\text{s} \ 2}}{1 - \varphi_{\text{eq}}} - 2\chi_0(T)\varphi_{\text{eq}}^{\text{s} \ 2} - 3\chi_1\varphi_{\text{eq}}^{\text{s} \ 3} + \beta_1(1 - c_t)\varphi_{\text{eq}}^{\text{s}} + \beta_1c_t\varphi \right] + c_0 \left[\frac{\varphi_{\text{eq}}^{\text{s}}}{2\varphi_0} - \frac{1}{3} \left(\frac{\varphi_{\text{eq}}^{\text{s}}}{\varphi_0} \right)^{1/3} \right]$$
(Equation 10)

and

$$G = c_0 \left(\varphi_{\text{eq}} / \varphi_0 \right)^{1/3}$$
 (Equation 11)

Both expressions in Equations 10 and 11 are normalized by k_BTN_A/V_s and $\varphi_{\rm eq}^s$ is given by solving Equation 8.